Chapter

MHD Flow and Heat Transfer of Casson Nanofluid through a Porous Media over a Stretching Sheet

Ayesha Siddiqui and Bandari Shankar

Abstract

The present chapter aims at investigating the magnetohydrodynamic (MHD) boundary layer flow and heat transfer of a non-Newtonian fluid over a stretching surface through a porous medium. Casson fluid model is utilized to describe the non-Newtonian fluid behavior. Two types of nanofluids, that is, Ag-water and Cu-water, are studied. The governing partial differential equations are transformed into a system of coupled non-linear ordinary differential equations using similarity transformations and then solved numerically using the Keller box method. Numerical results are obtained for the velocity, temperature, skin friction coefficient and Nusselt number. The influence of the various governing parameters viz. Casson parameter, magnetic parameter, porosity parameter and Prandtl number on the flow and heat transfer characteristics of the nanofluids is plotted graphically and discussed in detail. The chapter shows that with an increase in the Casson parameter, the velocity field decreases whereas the temperature profile increases. A decrease in the momentum boundary layer thickness and an increase in the thermal boundary layer thickness are noted with an increase in the magnetic parameter.

Keywords: magnetohydrodynamic, Casson fluid, porous medium, stretching sheet

1. Introduction

The boundary layer flow and heat transfer over a stretching sheet have momentous views not only from theoretical point of view but also one can see their practical applications in the paper production, polymer industry, crystal growing, food processing etc. Crane [1] was the first to study the boundary layer flow yielded by a stretching sheet. He gave an exact solution for the originating problem. Later on, the boundary layer flow over linear and non-linear stretching surfaces have pulled in a great deal of interest of many of the researchers [2–5]. Magnetohydrodynamic (MHD) boundary layer flow due to an exponentially stretching sheet with radiation effect has been examined by Ishak [6]. In fluid dynamics, the influence of external magnetic field on magnetohydrodynamic (MHD) flow over a stretching sheet is very significant due to its applications in many engineering problems such as for purification of crude oil, paper production and glass manufacturing. A physiological process in human body can be deciphered by processes like MRI, NMRI

and MRT, in which MHD plays an important role [7, 8]. Pavlov [9] analyzed the effect of external magnetic field on MHD flow over a stretching sheet. Andersson [10] studied the MHD flow of viscous fluid over a stretching sheet. A robust numerical method for solving stagnation point flow over a permeable shrinking sheet under the influence of MHD was considered by Bhatti et al. [11]. They observed that as the Hartman number increases, the fluid velocity also increases. Sheikholeslami et al. [12] employed the control volume-based finite element method (CVFEM) to show the influence of external magnetic source on $Fe_3O_4 - H_2O$ nanofluid behavior in a permeable cavity considering shape effect. They remarked that the nanofluid velocity and heat transfer rate decrease with augment of Hartmann number. The rate of heat transfer between the stretching surface and the fluid flow is crucial to obtain the desired quality of the end product. So, in the boundary layer flow problems dealing with the non-Newtonian fluids, heat transfer analysis plays an important role. Barzegar et al. [13] applied neural network for the estimation of heat transfer treatment of $Al_2O_3 - H_2O$ nanofluid through a channel. Sadoughi et al. [14] investigated CuO-water nanofluid heat transfer enhancement in the presence of melting surface. Sheikholeslami et al. [15] investigated nanofluid heat transfer augmentation and exergy loss inside a pipe equipped with innovative turbulators. Sheikholeslami et al. [16] investigated thermal radiation of ferrofluids in the presence of Lorentz force considering variable viscosity and reported that the Nusselt number increases with an increase of buoyancy forces and radiation parameter, but it is reduced with rise of Hartmann number. For an appraisal of technological applications, knowledge of the rheological characteristics of the non-Newtonian fluids [17] is required. In the study of fluid dynamics and heat transfer, an essential component is the fundamental analysis of the non-Newtonian fluid flow field in a boundary layer adjacent to a stretching sheet or an extended surface [18–20]. The flows of various non-Newtonian fluids over stretching or shrinking sheets were analyzed by Liao [21], Hayat et al. [22] and Ishak et al. [23]. Compared to the viscous fluids, the characteristics of the non-Newtonian fluids are different and the governing equations are also extremely nonlinear and complicated. Therefore, no single constitutive equation, displaying all properties of such fluids is available [24, 25]. In literature, several models of non-Newtonian fluids have been proposed but most of the models are related with simple models like "the power-law fluid of grade two or three" [26–30]. Casson fluid model is a non-Newtonian fluid model. A Casson fluid can be defined as a shear thinning liquid which is assumed to have an infinite viscosity at zero rate of shear and a zero viscosity at an infinite rate of shear [31]. Examples of Casson fluid are jelly, tomato sauce, honey, soap and concentrated fruit juices. Human blood is also an example of Casson fluid. Rouleaux is a chain-like structure formed by the human red blood cells, due to the presence of substances like globulin, protein and fibrinogen in an aqueous base plasma. If the rouleaux acts like a plastic solid, then there exists a yield stress that can be identified with the constant yield stress in Casson fluid [32]. Casson fluid model (McDonald 1974) [33] describes the blood flow through small vessels at low shear rates. Mukhopadhyay [34] examined the effects of Casson fluid flow and heat transfer over a non-linearly stretching surface. She concluded that temperature increases with an increase in non-linear stretching parameter and the momentum boundary layer thickness decreases with an increase in Casson parameter. The relationship between the fluxes and the driving potentials becomes complicated whenever heat and mass transfer occur simultaneously in a moving fluid. Apart from the temperature gradients, the concentration gradients are also one of the factors to cause energy flux. The generation of energy flux by concentration gradient is named as diffusion-thermo(Dufour) effect and that of mass flux by temperature gradient is termed as thermal-diffusion(Soret) effect. Hayat et al. [35] and Nawaz et al. [36] studied Soret and Dufour effects on the MHD flow of a Casson fluid on a stretching

surface. An analysis on heat and mass transfer in stagnation point flow of a polar fluid toward a stretching surface in porous medium in the presence of Soret, Dufour and chemical reaction effects was carried out by Chamkha and Aly [37]. They observed that as the Soret number increases and the Dufour number decreases, the fluid velocity increases. Casson [38] derived the non-linear Casson constitutive equation and it depicts the properties of many polymers. Mustafa et al. [39] studied the stagnation point flow and heat transfer in a Casson fluid flow over a stretching sheet. An exact solution of the steady boundary layer flow of a Casson fluid over a porous stretching sheet was studied by Shehzad et al. [40].

In a boundary layer flow, the flow field gets significantly affected by the presence of porous media and as a result, the rate of heat transfer at the surface also gets influenced. Practical applications of the flow and heat transfer through a porous media can be seen in geophysical fluid dynamics such as limestone, wood, beach sand, sandstone, the human lungs and in small blood vessels [41]. Sheikholeslami [42] analyzed the exergy and entropy of nanofluids under the impact of Lorentz force through a porous media by incorporating the CVFEM method. He observed that exergy drop diminishes with reduction of magnetic forces. Shehzad et al. [43] simulated nanofluid convective flow inside a porous enclosure by means of a two-temperature model. They remarked that the porosity and temperature gradient are inversely related. Sheikholeslami [44] studied CuO-water nanofluid flow due to magnetic field inside a porous media considering Brownian motion. Shehzad et al. [45] considered the numerical modeling for alumina nanofluid's magnetohydrodynamic convective heat transfer in a permeable medium using Darcy law. They concluded that an increase in radiation parameter makes the thermal boundary layer thinner. Sheikholeslami [46] examined CuO-water nanofluid's free convection in a porous cavity considering the Darcy law. He applied the CVFEM method to interpret his results. Numerical simulation for heat transfer intensification of a nanofluid in a porous curved enclosure considering shape effect of Fe_3O_4 nanoparticles was carried out by Shamlooei et al. [47]. Rokni et al. [48] made a numerical simulation for the impact of Coulomb force on nanofluid heat transfer in a porous enclosure in the presence of thermal radiation. They noticed that the Nusselt number of nanoparticles with platelet shape is the highest. Sibanda et al. [49] considered nanofluid flow over a non-linear stretching sheet in porous media with MHD and viscous dissipation effects. Sheikholeslami et al. [50] examined magnetohydrodynamic nanofluid convection in a porous enclosure considering heat flux boundary condition. Their studies reveal that the temperature gradient shows a reduction with increasing values of Hartman number. The objective of this chapter is to study the MHD flow and heat transfer of a Casson nanofluid through a porous medium over a stretching sheet. The governing partial differential equations of the flow and energy distribution are transformed into a set of non-linear ordinary differential equations by using similarity transformations and are then solved numerically by a finite difference numerical technique called Keller box method [51]. The effects of various governing parameters on the flow and heat transfer characteristics of the nanofluids, that is, Ag-water and Cu-water are analyzed and shown graphically.

2. Equations of motion

Consider the steady two-dimensional MHD flow of an electrically conducting non-Newtonian Casson nanofluid over a stretching sheet situated at $y = 0$. The flow is confined in the region $y>0$. Two equal and opposite forces are applied along the

x-axis so that the wall is stretched with the origin fixed. The rheological equation of state for an isotropic and incompressible flow of the Casson nanofluid is

$$\tau_{ij} = \begin{cases} 2\left(\mu_B + \dfrac{P_y}{\sqrt{2\pi}}\right)e_{ij} & \pi > \pi_c \\ 2\left(\mu_B + \dfrac{P_y}{\sqrt{2\pi_c}}\right)e_{ij} & \pi < \pi_c \end{cases} \tag{1}$$

$\pi = e_{ij}e_{ij}$ *and* e_{ij} is the (i,j)th component of deformation rate, n is the product of deformation rate with itself, π_c is a critical value of this product based on the non-Newtonian model, μ_B is the plastic dynamic viscosity of the non-Newtonian fluid and P_y is the yield stress of the fluid. The continuity, momentum and energy equations governing such type of flow are

$$\frac{\partial u}{\partial x} + \frac{\partial v}{\partial y} = 0 \tag{2}$$

$$u\ \frac{\partial u}{\partial x} + v\ \frac{\partial u}{\partial y} = \nu_{nf}\left(1 + \frac{1}{\gamma}\right)\ \frac{\partial^2 u}{\partial y^2} - \left(\frac{\sigma B_0^2}{\rho_{nf}} + \frac{\nu_{nf}}{k_0}\right)u \tag{3}$$

$$u\ \frac{\partial T}{\partial x} + v\ \frac{\partial T}{\partial y} = \alpha_{nf}\ \frac{\partial^2 T}{\partial y^2} \tag{4}$$

where u and v are the velocity components in the x and y directions, respectively. ν_{nf} is the kinematic viscosity, ρ_{nf} is the Casson fluid density, $\gamma = \mu_B\sqrt{\frac{2\pi_c}{P_y}}$ is the parameter of Casson fluid, σ is the electrical conductivity of the fluid, α_{nf} is the thermal diffusivity, T is the temperature and k_0 is the permeability of the porous medium.

The appropriate boundary conditions for the problem are given by

$$\begin{aligned} u = u_w = bx, \qquad v = 0 & \\ T = T_w = T_\infty + A\left(\tfrac{x}{l}\right)^2 & \quad \text{at} \quad y = 0 \\ u \to 0, \qquad T \to T_\infty & \quad \text{as} \quad y \to \infty \end{aligned} \tag{5}$$

where u_w = bx, b>0, is the stretching sheet velocity and A is a constant, l is the characteristic length, T is the temperature of the fluid, T_w is the temperature of the sheet and T_∞ is the free stream temperature.

Introducing the following similarity transformations

$$\begin{aligned} \eta = y\sqrt{\frac{b}{\nu_f}}, \quad u = bxf'(\eta) \\ v = -\sqrt{b\nu_f}\,f(\eta), \quad \theta = \frac{T - T_\infty}{T_w - T_\infty} \end{aligned} \tag{6}$$

Making use of Eq. (6), the governing equations (3) and (4) are reduced into the non-dimensional form as follows

$$\left(1 + \frac{1}{\gamma}\right)f''' + \phi_1\left(ff'' - f'^2 - \frac{M}{\phi_2}f'\right) - kf' = 0 \tag{7}$$

$$\theta'' + \left(\frac{k_f}{k_{nf}}\Pr\phi_3\right)f\theta' = 0 \tag{8}$$

The corresponding boundary conditions are

$$\begin{aligned} f = 0, \quad f' = 1, \quad \theta = 1 \qquad & \text{at} \quad \eta = 0 \\ f' \to 0, \quad \theta \to 0 \qquad & \text{as} \quad \eta \to \infty \end{aligned} \tag{9}$$

where prime denotes differentiation with respect to η, M = $\frac{\sigma B_0^2}{b\rho_f}$ is the magnetic parameter, $k = \frac{\nu_f}{bk_0}$ is the porosity parameter and Pr = $\frac{\nu_f}{\alpha_f}$ is the Prandtl number.

The important physical quantities of interest are the skin friction coefficient C_f and the local Nusselt number Nu_x defined as

$$C_f = \frac{\tau_w}{\rho_f u_w^2} \qquad and \qquad Nu_x = \frac{x\, q_w}{k\,(T_w - T_\infty)} \tag{10}$$

where τ_w is the skin friction or the shear stress along the stretching surface and q_w is the surface heat flux given by

$$\tau_w = \left(\mu_B + \frac{P_y}{\sqrt{2\,\pi_c}}\right)\left(\frac{\partial u}{\partial y}\right)_{y=0} \qquad and \qquad q_w = -k_{nf}\left(\frac{\partial T}{\partial y}\right)_{y=0} \tag{11}$$

Substituting the transformations in (6) in equations (10) and (11), we obtain

$$C_f\ \mathrm{Re}_x^{\frac{1}{2}} = \left(1 + \frac{1}{\gamma}\right) f''(0) \qquad and \qquad Nu_x\ (\mathrm{Re}_x)^{\frac{-1}{2}} = -\theta'(0) \tag{12}$$

where $Re_x = \frac{u_w^2\, x}{\nu}$ is the local Reynolds number.

3. Numerical solution

A finite difference scheme known as Keller box method is used to solve numerically the system of non-linear ordinary differential equations (7) and (8) together with the boundary conditions in (9). The method was developed by Keller [51] and is described in Cebeci and Bradshaw [52]. The main steps involved in this method are:

1. Reduce the governing equations of the problem to a system of first-order ordinary differential equations.

2. Convert the resulting system of first-order ordinary differential equations into difference equations by using the central difference scheme.

3. Newton's method is used to linearize the non-linear finite difference equations so obtained and then write them in matrix-vector form.

4. Solve the linearized system of difference equations by using the block tri-diagonal elimination technique.

The method is highly adaptable to solve non-linear problems. In this method, the choice of the initial guess is very important to give the most accurate solution to the problem and it is made based on the convergence criteria along with the boundary conditions of the flow into consideration. In boundary layer flow calculations, the

greatest error appears in the wall shear stress, as mentioned in Cebeci and Bradshaw [52]. So, in accordance with it, the values of the wall shear stress, in our case $f''(0)$ is commonly used as a convergence criteria. We used this convergence criterion in the present chapter. A convergence criteria of 10^{-4} is chosen which gives about a four decimal places accuracy for most of the prescribed quantities.

4. Results and discussion

In order to analyze the results, numerical computation has been carried out to calculate the velocity profiles, temperature profiles, skin friction coefficient and local Nusselt number for various values of the parameters that describe the flow characteristics, that is, magnetic parameter (M), Casson parameter (γ), porosity parameter (k) and nanoparticle volume fraction (ϕ). The numerical results are presented graphically in **Figures 1–9**. To know the accuracy of the applied numerical scheme, a comparison of the present results corresponding to the values of the skin friction coefficient $-f''(0)$ for various values of M and ϕ when Prandtl number Pr = 6.2 is made with the available results of Hamad [53] and presented in **Table 1**. It is observed that as M and ϕ increase, the skin friction coefficient also increases. This is due to the fact that an increase in M results in an increase in Lorentz force which opposes the motion of flow. A comparison of the numerical results of the local Nusselt number $-\theta'(0)$ is also done with Vajravelu [54] for various values of the Prandtl number Pr and presented in **Table 2**. It is clear from **Table 2** that the heat transfer rate coefficient increases with an increase in Prandtl number, which is the ratio of momentum diffusivity to thermal diffusivity. So, as Prandtl number increases, the momentum diffusivity increases whereas the thermal diffusivity decreases. Hence, the rate of heat transfer at the surface increases with increasing values of Pr. The results are found to be in excellent agreement. **Figure 1** shows the effects of Casson parameter γ on the velocity profile $f'(\eta)$, that is, $f'(\eta)$ is a decreasing function of γ. The momentum boundary layer thickness decreases with an increase in γ, because as the Casson parameter γ increases, the yield stress decreases and as a result the velocity of the fluid is suppressed and the reverse can be seen in **Figure 2**, which shows the effects of Casson parameter γ on the temperature profile $\theta(\eta)$. It can be seen that the temperature of the nanofluids is enhanced with the increasing values of γ and hence the thermal boundary layer thickness increases as the elasticity stress parameter is increased. **Figure 3** illustrates the effects of

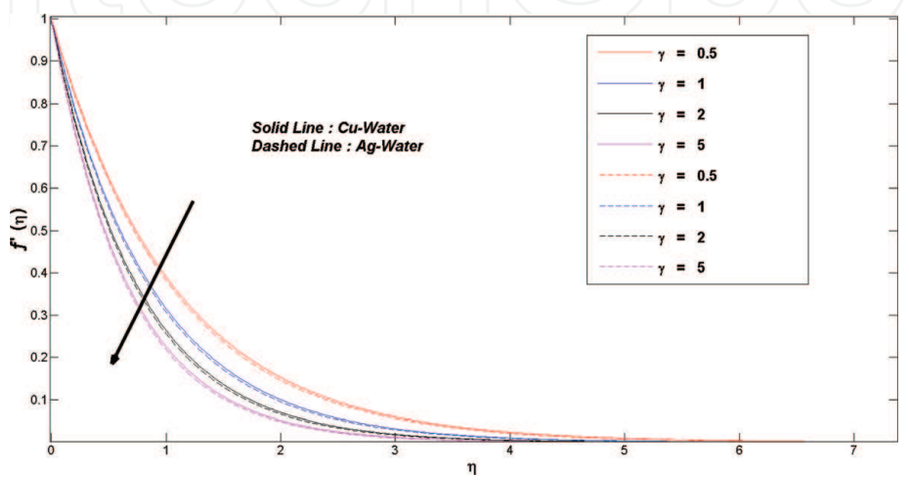

Figure 1.
Velocity profiles $f'(\eta)$ for various values of γ with $M = 1$, $k = 0.5$, $\phi = 0.1$ and $\Pr = 6.2$.

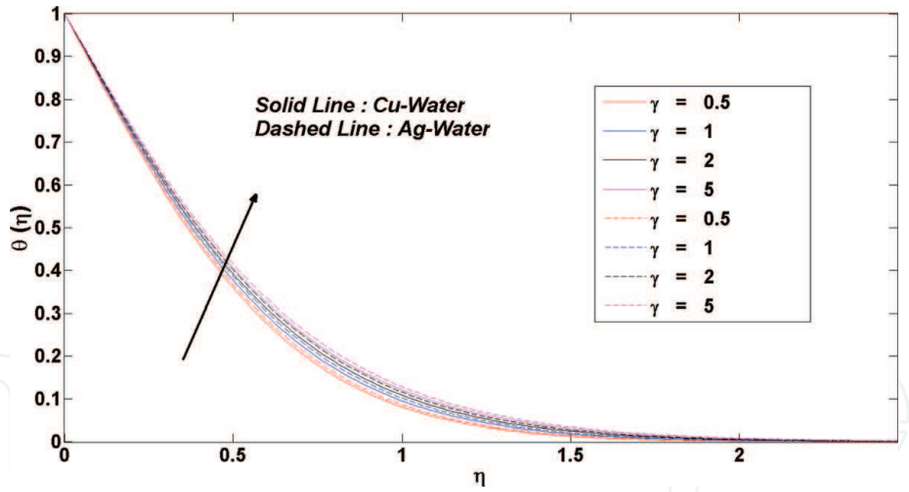

Figure 2.
Temperature profiles $\theta(\eta)$ for various values of γ with $M = 1$, $k = 0.5$, $\phi = 0.1$ and $\Pr = 6.2$.

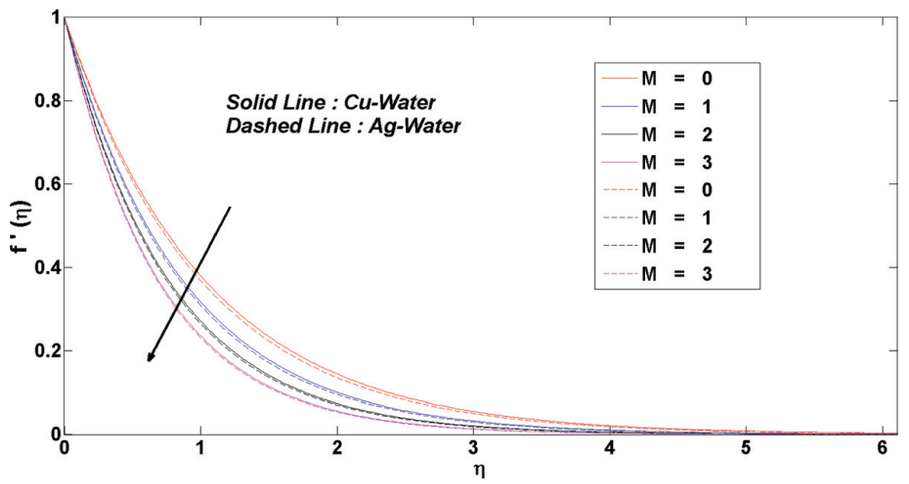

Figure 3.
Velocity profiles $f'(\eta)$ for various values of M with $\gamma = 1$, $k = 0.5$, $\phi = 0.1$ and $\Pr = 6.2$.

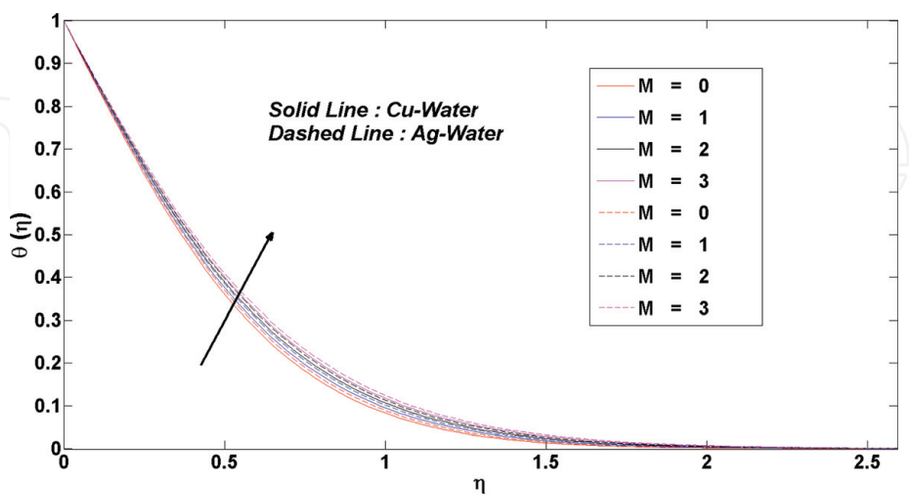

Figure 4.
Temperature profiles $\theta(\eta)$ for various values of M with $\gamma = 1$, $k = 0.5$, $\phi = 0.1$ and $\Pr = 6.2$.

magnetic parameter M on the velocity distribution. From the figure, we can observe that as 'M' increases, the fluid velocity decreases. This is because Lorentz force is induced by the transverse magnetic field and it opposes the motion of the fluid.

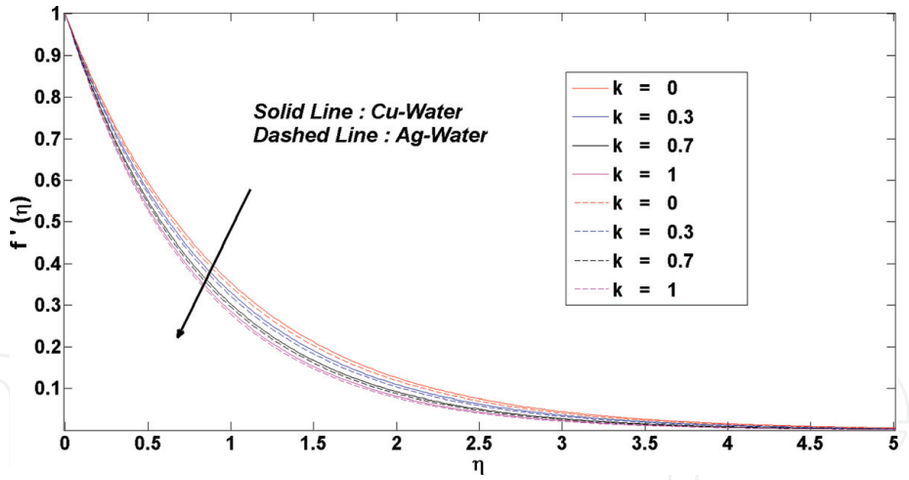

Figure 5.
Velocity profiles $f'(\eta)$ for various values of k with $M = 1, \gamma = 1, \ \phi = 0.1$ and $\Pr = 6.2$.

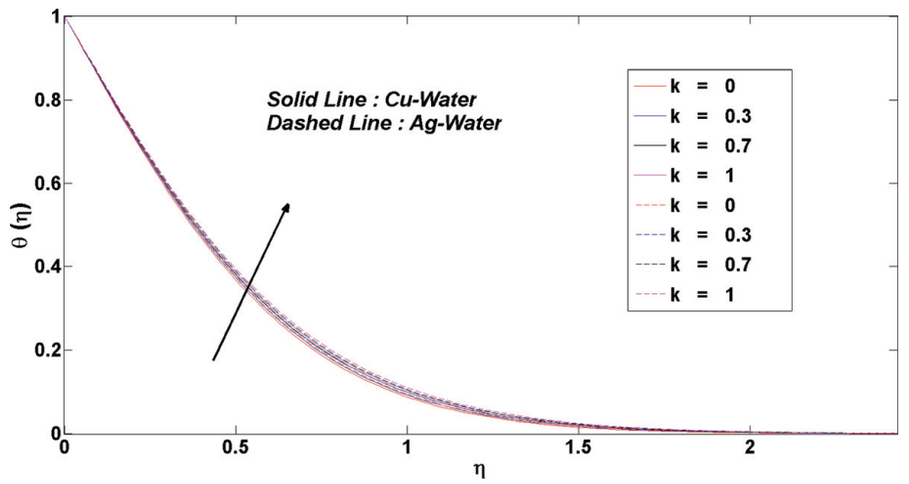

Figure 6.
Temperature profiles $\theta(\eta)$ for various values of k with $M = 1, \gamma = 1, \ \phi = 0.1$ and $\Pr = 6.2$.

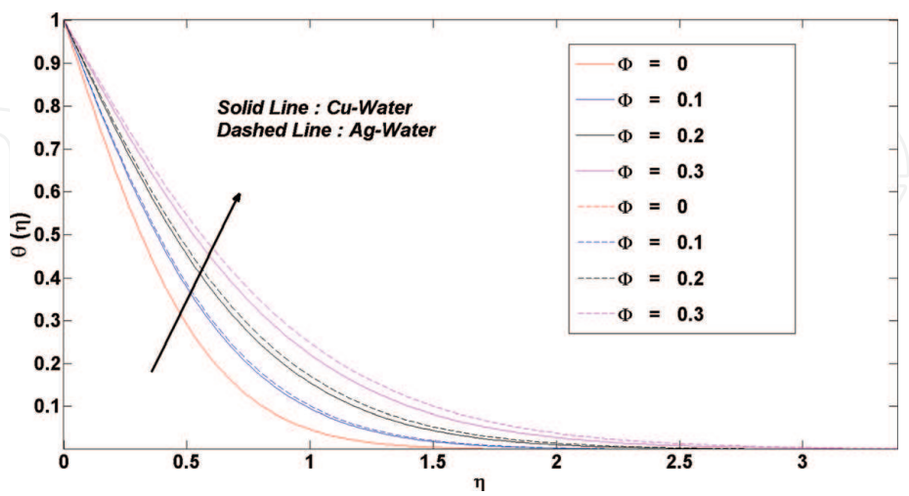

Figure 7.
Temperature profiles $\theta(\eta)$ for various values of ϕ with $\gamma = 1, \ \Pr = 6.2, \ M = 1$ and $k = 0.5$.

As the magnetic parameter M increases, the momentum boundary layer thickness decreases. The velocity distribution in the case of Cu-water nanofliud is higher as compared to Ag-water nanofluid and **Figure 4** shows the effect of magnetic parameter 'M' on the temperature profile $\theta(\eta)$. As 'M' increases, the thermal

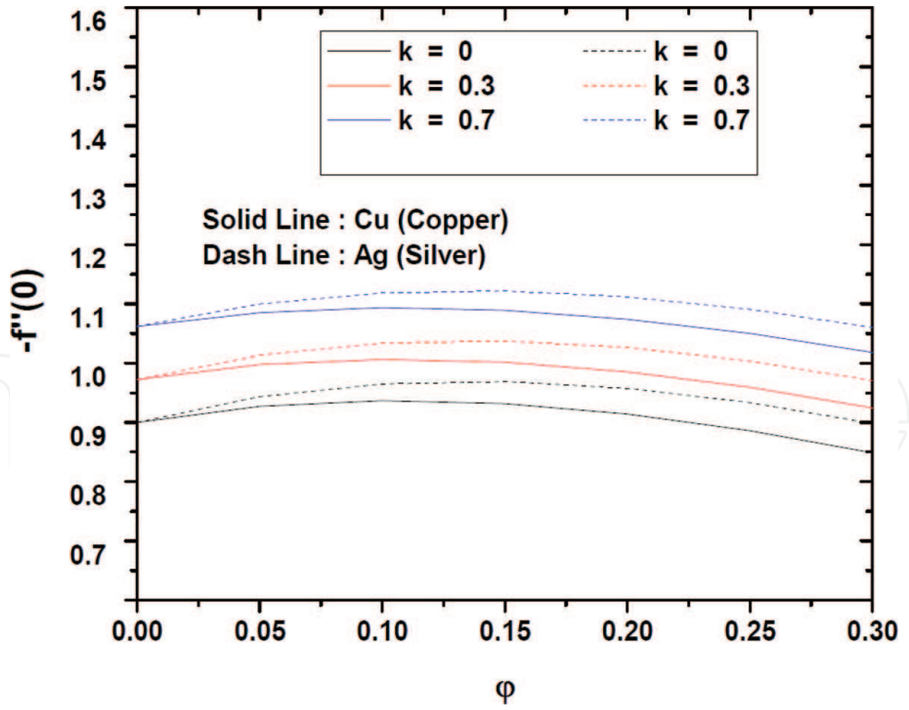

Figure 8.
Variation of skin friction coefficient $-f''(0)$ with nanoparticle volume fraction ϕ for various values of porosity parameter k.

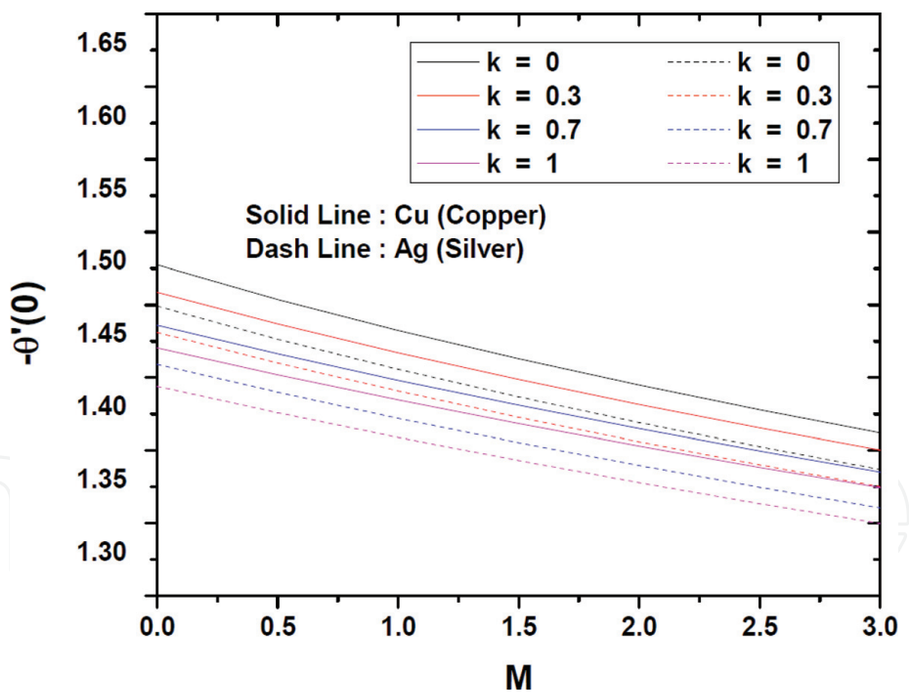

Figure 9.
Variation of heat transfer coefficient $-\theta'(0)$ with magnetic parameter M for various values of porosity parameter k.

boundary layer thickness also increases since the presence of magnetic field enhances the fluid's temperature within the boundary layer. The Ag-water nanofluid has a thicker thermal boundary layer than the Cu-water nanofluid because the thermal conductivity of Ag is more than that of Cu. **Figure 5** shows the effects of porosity parameter k on the velocity distribution. It is observed that with the increasing values of k, the velocity field decreases. The fluid velocity decreases because the presence of a porous medium increases the resistance to flow. In the

		Cu-Water		Ag-Water	
M	Φ	**Hamad [53]**	**Present**	**Hamad [53]**	**Present**
0	0.05	1.10892	1.1089	1.13966	1.1397
	0.1	1.17475	1.1747	1.22507	1.2251
	0.15	1.20886	1.2089	1.27215	1.2722
	0.2	1.21804	1.2180	1.28979	1.2898
0.5	0.05	1.29210	1.2921	1.31858	1.3186
	0.1	1.32825	1.3282	1.37296	1.3730
	0.15	1.33955	1.3396	1.39694	1.3969
	0.2	1.33036	1.3304	1.39634	1.3963
1	0.05	1.45236	1.4524	1.47597	1.4760
	0.1	1.46576	1.4658	1.50640	1.5064
	0.15	1.45858	1.4586	1.51145	1.5115
	0.2	1.43390	1.4339	1.49532	1.4953
2	0.05	1.72887	1.7289	1.74875	1.7487
	0.1	1.70789	1.7079	1.74289	1.7429
	0.15	1.67140	1.6714	1.71773	1.7177
	0.2	1.62126	1.6213	1.67583	1.6758

Table 1.
Comparison of results of the skin friction coefficient $-f''(0)$ for various values of M and ϕ.

Pr	**Vajravelu [54]**	**Present**
0.72	0.4590	0.4596
7	1.8953	1.8954

Table 2.
Comparison of values of local Nusselt number $-\theta'(0)$ for various values of Pr.

case of Ag-water nanofluid, the velocity is slightly less as compared with Cu-water nanofluid. **Figure 6** illustrates the impact of the porosity parameter k on the temperature profile and it is noted that with the increasing values of the porosity parameter, the temperature of the fluid increases. The temperature of Ag-water nanofluid is more as compared with Cu-water nanofluid. **Figure 7** shows the effect of nanoparticle volume fraction ϕ on the temperature of the nanofluids. From the figure, it is clear that the fluid temperature increases as the nanoparticle's volume fraction ϕ increases. The temperature distribution in Ag-water nanofluid is higher than that of Cu-water nanofluid. It is also observed that as the nanoparticle volume fraction increases, the thermal boundary layer thickness increases because as volume fraction increases, the thermal conductivity of the fluid increases. **Figure 8** shows the effect of the porosity parameter k and the nanoparticle volume fraction ϕ on the wall skin friction. It is observed that the skin friction increases with the increase in the porosity parameter k and the nanoparticle volume fraction ϕ for both the Cu-water and Ag-water nanofluids. The wall skin friction is higher in the case of Ag-water nanofluid than in Cu-water. Hence, the Ag-water nanofluid gives a higher drag in opposition to the flow than the Cu-water nanofluid. **Figure 9** shows the effect of the magnetic parameter M and porosity parameter k on the wall heat

transfer rate $-\theta'(0)$. The influence of the magnetic field is to reduce the wall heat transfer rate. The porous media effect reduces the wall heat transfer rate. Moreover, the rate of heat transfer at the wall is less in the case of the Ag-water nanofluid as compared with Cu-water nanofluid.

5. Conclusion

MHD flow and heat transfer of Casson nanofluid through a porous medium over a stretching sheet have been investigated. The governing boundary layer equations are transformed into ordinary differential equations using similarity transformations and are then solved by the Keller box method. The effects of the various governing parameters viz. magnetic parameter M, Casson parameter γ, porosity parameter k and the nanoparticle volume fraction ϕ on the flow and heat transfer characteristics of two types of nanofluids, that is, Ag-water and Cu-water are determined [55, 56]. The present chapter leads to the following observations:

1. An increase in the Casson parameter γ suppresses the velocity field of the nanofluids whereas the temperature is enhanced.

2. With an increase in the magnetic parameter M, the momentum boundary layer thickness decreases while the thermal boundary layer thickness increases.

3. The temperature and the thermal boundary thickness increase as the nanoparticle volume fraction ϕ increases.

4. Ag-water nanofluid has thicker thermal boundary layer than Cu-water nanofluid.

5. The velocity of the nanofluids decreases as the porosity parameter k increases and the reverse is observed in the case of temperature.

6. The skin friction increases with an increase in nanoparticle volume fraction ϕ and the porosity parameter k.

7. The rate of heat transfer at the surface of the sheet decreases with an increase in magnetic parameter M and porosity parameter k.

Nomenclature

C_f	skin friction coefficient
C_p	specific heat capacity at constant pressure
f	dimensionless velocity
k_f	thermal conductivity of the base fluid
k_s	thermal conductivity of the nanoparticle
k_{nf}	thermal conductivity of the nanofluid
k^*	mean absorption coefficient
l	characteristic length
k_0	permeability of the porous medium
M	magnetic field parameter
Nu_x	local Nusselt number

Pr	Prandtl number
P_y	yield stress of the fluid
q_w	heat flux
Re_x	local Reynolds number
T	fluid temperature
T_w	temperature at the stretching surface
T_∞	temperature of the fluid far away from the stretching surface
u, v	velocity components along x-axis and y-axis, respectively
u_w	velocity of the stretching surface
x, y	Cartesian coordinates measured along stretching surface
π	product of the component of deformation rate with itself
π_c	critical value of the product
α_{nf}	thermal diffusivity of the nanofluid
γ	Casson fluid parameter
η	dimensionless similarity variable
σ	electrical conductivity
θ	dimensionless temperature
ϕ	nanoparticle volume fraction
τ_w	shear stress
μ_f	dynamic viscosity of the base fluid
μ_{nf}	dynamic viscosity of the nanofluid
ν_f	kinematic viscosity of the base fluid
ν_{nf}	kinematic viscosity of the nanofluid
ρ_f	density of the base fluid
ρ_s	density of the nanoparticle
ρ_{nf}	density of the nanofluid
$(\rho c_p)_f$	heat capacity of the base fluid
$(\rho c_p)_s$	heat capacity of the nanoparticle
$(\rho c_p)_{nf}$	heat capacity of the nanofluid
μ_B	plastic dynamic viscosity of the fluid
$'$	denotes differentiation with respect to η

Author details

Ayesha Siddiqui[1*] and Bandari Shankar[2]

1 Department of Mathematics, Nizam College, OU, Hyderabad, Telangana, India

2 Department of Mathematics, Osmania University, Hyderabad, Telangana, India

*Address all correspondence to: ayesha_siddiquias@yahoo.com

References

[1] Crane LJ. Flow past a stretching plate. Journal of Applied Mathematics and Physics. 1970;**21**:645-647

[2] Cortell R. Effects of viscous dissipation and work done by deformation on the MHD flow and heat transfer of a viscoelastic fluid over a stretching sheet. Physics Letters A. 2006;**357**:298-305

[3] Bhattacharyya K, Hayat T, Alsaedi A. Analytic solution for magnetohydrodynamic boundary layer flow of Casson fluid over a stretching/shrinking sheet with wall mass transfer. Chinese Physics B. 2013;**22**

[4] Mukhopadhyay S. Casson fluid flow and heat transfer over a nonlinearly stretching surface. Chinese Physics B. 2013;**22**

[5] Rashidi MM, Mohimanian Pour SA. Analytic approximate solutions for unsteady boundary-layer flow and heat transfer due to a stretching sheet by homotopy analysis method. Nonlinear Analysis: Modelling and Control. 2010;**15**:83-95

[6] Ishak A. MHD boundary layer flow due to an exponentially stretching sheet with radiation effect. Sains Malaysiana. 2011;**40**:391-395

[7] Bachok N, Ishak A, Pop I. Boundary-layer flow of nanofluids over a moving surface in a flowing fluid. International Journal of Thermal Sciences. 2010;**49**:1663-1668

[8] Mandal IC, Mukhopadhyay S. Heat transfer analysis for fluid flow over an exponentially stretching porous sheet with surface heat flux in porous medium. Ain Shams Engineering Journal. 2013;**4**:103-110

[9] Pavlov KB. Magneto hydrodynamic flow of an incompressible viscous fluid caused by the deformation of a plane surface. Magneto Hydrodynamics. 1974;**10**:146-148

[10] Andersson HI. MHD flow of a viscoelastic fluid past a stretching surface. Acta Mechanica. 1992;**95**:227-230

[11] Bhatti MM, Abbas MA, Rashidi MM. A robust numerical method for solving stagnation point flow over a permeable shrinking sheet under the influence of MHD. Applied Mathematics and Computation. 2018;**316**:381-389

[12] Sheikholeslami M, Shehzad SA. CVFEM for influence of external magnetic source on $Fe_3O_4 - H_2O$ nanofluid behavior in a permeable cavity considering shape effect. International Journal of Heat and Mass Transfer. 2017;**115**:180-191

[13] Sheikholeslami M, Barzegar Gerdroodbary M, Moradi R, Shafee A, Li Z. Application of neural network for estimation of heat transfer treatment of $Al_2O_3 - H_2O$ nanofluid through a channel. Computer Methods in Applied Mechanics and Engineering. 2019;**344**:1-12

[14] Sheikholeslami M, Sadoughi MK. Simulation of CuO-water nanofluid heat transfer enhancement in presence of melting surface. International Journal of Heat and Mass Transfer. 2018;**116**:1-12

[15] Sheikholeslami M, Jafaryar M, Saleem S, Li Z, Shafee A, Jiang Y. Nanofluid heat transfer augmentation and exergy loss inside a pipe equipped with innovative turbulators. International Journal of Heat and Mass Transfer. 2018;**126**:156-163

[16] Sheikholeslami M, Shehzad SA. Thermal radiation of ferrofluid in existence of Lorentz forces considering

variable viscosity. International Journal of Heat and Mass Transfer. 2017;**109**: 82-92

[17] Abel MS, Mahesha N. Heat transfer in MHD viscoelastic fluid flow over a stretching sheet with variable thermal conductivity, non-uniform heat source and radiation. Applied Mathematical Modeling. 2008;**32**:1965-1983

[18] Hsiao KL. Conjugate heat transfer of magnetic mixed convection with radiative and viscous dissipation effects for second-grade viscoelastic fluid past a stretching sheet. Applied Thermal Engineering. 2007;**27**:1895-1903

[19] Mukhopadhyay S. Heat transfer analysis of the unsteady flow of a maxwell fluid over a stretching surface in the presence of a heat source/sink. Chinese Physics Letters. 2012;**29**

[20] Mukhopadhyay S, Bhattacharyya K. Unsteady flow of a Maxwell fluid over a stretching surface in presence of chemical reaction. Journal Egyptian Math. 2012;**20**:229-234

[21] Liao SJ. On the analytic solution of magnetohydrodynamic flows of non-Newtonian fluids over a stretching sheet. Journal of Fluid Mechanics. 2003; **488**:189-212

[22] Hayat T, Javed T, Sajid M. Analytic solution for MHD rotating flow of a second grade fluid over a shrinking surface. Physics Letters A. 2008;**372**: 3264-3273

[23] Ishak A, Lok Y, Pop I. Non-Newtonian power-law fluid flow past a shrinking sheet with suction. Chemical Engineering Communications. 2012; **199**:142-150

[24] Mukhopadhyay S. Upper-convected Maxwell fluid flow over an unsteady stretching surface embedded in porous medium subjected to suction/blowing. Zeitschrift fr Naturforschung A A, Journal of Physical Sciences. 2012;**67**: 641-646

[25] Mukhopadhyay S, Vajravelu K. Effects of transpiration and internal heat generation/absorption on the unsteady flow of a Maxwell fluid at a stretching surface. The American Society of Mechanical Engineers Journal of Applied Mechanics. 2012;**79**

[26] Andersson HI, Bech KH, Dandapat BS. Magnetohydrodynamic flow of a power-law fluid over a stretching sheet. International Journal of Non-Linear Mechanics. 1992;**7**:929-936

[27] Hassanien I. A, mixed convection in micropolar boundary-layer flow over a horizontal semi-infinite plate. The American Society of Mechanical Engineers Journal of Fluids Engineering. 1996;**118**:833-838

[28] Haroun MH. Effect of Deborah number and phase difference on peristaltic transport of a third-order fluid in an asymmetric channel. Communications in Nonlinear Science and Numerical Simulation. 2007;**12**: 1464-1480

[29] Siddiqui AM, Zeb A, Ghori QK, Benharbit AM. Homotopy perturbation method for heat transfer flow of a third grade fluid between parallel plates. Chaos, Solitons & Fractals. 2008;**36**:182-192

[30] Sajid M, Ahmad I, Hayat T, Ayub M. Unsteady flow and heat transfer of a second grade fluid over a stretching sheet. Communications in Nonlinear Science and Numerical Simulation. 2009;**14**:96-108

[31] Dash RK, Mehta KN, Jayaraman G. Casson fluid flow in a pipe filled with a homogeneous porous medium. International Journal of Engineering Science. 1996;**34**:1145-1156

[32] Fung YC. Biodynamics Circulation. Springer Verlag; 1984

[33] McDonald DA. Blood flows in arteries. Edward Arnold; 1974

[34] Casson MS. Fluid flow and heat transfer over a nonlinearly stretching surface. Chinese Physics B. 2013;**22**: 577-585

[35] Hayat T, Shehzad SA, Alsaedi A, Alhothuali MS. Mixed convection stagnation point flow of Casson fluid with convective boundary conditions. Chinese Physics Letters. 2012;**29**

[36] Nawaz M, Hayat T, Alsaed A. Dufour and Soret effects on MHD flow of viscous fluid between radially stretching sheets in porous medium. Applied Mathematics and Mechanics. 2012;**33**:1403-1418

[37] Chamkha AJ, Aly AM. Heat and mass transfer in stagnation point flow of a polar fluid towards a stretching surface in porous media in the presence of Soret, Dufour and chemical reaction effects. Chemical Engineering Communications. 2010;**198**:214-234

[38] Casson N, Flow A. Equation for pigment-oil suspensions of the printing ink type. In: Mill CC, editor. Rheology of Disperse Systems. Oxford: Pergamon Press; 1959. pp. 84-104

[39] Mustafa M, Hayat T, Pop I, Hendi A. A Stagnation-point flow and heat transfer of a Casson fluid towards a stretching sheet. Zeitschrift fr Naturforschung A A Journal of Physical Sciences. 2012;**67**:70-76

[40] Shehzad SA, Hayat T, Qasim M, Asghar S. Efects of mass transfer on MHD flow of Casson fluid with chemical reaction and suction. Brazilian Journal of Chemical Engineering. 2013; **30**:187-195

[41] Khani F, Farmany A, Ahmadzadeh Raji M, Aziz A, Samadi F. Analytic solution for heat transfer of a third grade viscoelastic fluid in non-Darcy porous media with thermophysical effects. Brazilian Journal of Chemical Engineering Communications in Nonlinear Science and Numerical Simulation. 2009;**14**:3867-3878

[42] Sheikholeslami M. New computational approach for exergy and entropy analysis of nanofluid under the impact of Lorentz force through a porous media. Computer Methods in Applied Mechanics and Engineering. 2019;**344**:319-333

[43] Sheikholeslami M, Shehzad SA. Simulation of water based nanofluid convective flow inside a porous enclosure via non-equilibrium model. International Journal of Heat and Mass Transfer. 2018;**120**:1200-1212

[44] Sheikholeslami M. CuO-water nanofluid flow due to magnetic field inside a porous media considering Brownian motion. Journal of Molecular Liquids. 2018;**249**:921-929

[45] Sheikholeslami M, Shehzad SA, Li Z, Shafee A. Numerical modeling for alumina nanofluid magnetohydrodynamic convective heat transfer in a permeable medium using Darcy law. International Journal of Heat and Mass Transfer. 2018;**127**:614-622

[46] Sheikholeslami M. CuO-water nanofluid free convection in a porous cavity considering Darcy law. The European Physical Journal Plus. 2017; **132**:55

[47] Sheikholeslami M, Shamlooei M, Moradi R. Numerical simulation for heat transfer intensification of nanofluid in a porous curved enclosure considering shape effect of Fe_3O_4 nanoparticles. Chemical Engineering and Processing Process Intensification. 2018;**124**:71-82

[48] Sheikholeslami M, Rokni HB. Numerical simulation for impact of Coulomb force on nanofluid heat transfer in a porous enclosure in

presence of thermal radiation. International Journal of Heat and Mass Transfer. 2018;**118**:921-929

[49] Sibanda P, Khidir AA. Nanofluid flow over a nonlinear stretching sheet in porous media with MHD and viscous dissipation effects. Journal of Porous Media. 2014;**17**(5):391-403

[50] Sheikholeslami M, Shehzad SA. Magnetohydrodynamic nanofluid convection in a porous enclosure considering heat flux boundary condition. International Journal of Heat and Mass Transfer. 2017;**106**:1261-1269

[51] Keller HB. A New Difference Scheme for Parabolic Problems. Vol. 2. Academic Press; 1971. pp. 327-350

[52] Cebeci T, Bradshaw P. Physical and Computational Aspects of Convective Heat Transfer. Springer; 1988

[53] Hamad MAA. Analytical solution of natural convection flow of a nanofluid over a linearly stretching sheet in the presence of magnetic field. International Communications in Heat and Mass Transfer. 2011;**38**:487-492

[54] Vajravelu K. Viscous flow over a nonlinearly stretching sheet. Applied Mathematics and Computation. 2001; **124**:281-288

[55] Khan WA, Pop I. Free convection boundary layer flow past a horizontal flat plate embedded in a porous medium filled with a nanofluid. Journal of Heat Transfer. 2011;**133**

[56] Rashad AM, Reddy Gorla RS, Mansour MA, Ahmed SE. Free convection boundary layer flow past a horizontal flat plate embedded in a porous medium filled with a nanofluid. Journal of Heat Transfer. 2011;**133**:9